Interactions of vector solitons

Jianke Yang*
Department of Mathematics and Statistics, University of Vermont, 16 Colchester Avenue, Burlington, Vermont 05401
(Received 25 January 2001; published 18 July 2001)

In this paper, we study the interaction of two widely separated vector solitons in the nonintegrable coupled nonlinear Schrödinger (NLS) equations. Using a modification of Karpman-Solov'ev perturbation method, we derive dynamical equations for the evolution of both solitons' internal parameters. We show that these dynamical equations allow fixed points that correspond to stationary two-vector-soliton bound states if these solitons have the same phase in one component (same sign) and π-phase difference in the other component (opposite sign). However, linear stability analysis indicates that these bound states are always unstable due to a phase-related unstable eigenvalue. We also investigate vector-soliton interactions and show that, in contrast to soliton interactions in the single NLS equation, vector solitons repel or attract each other depending not only on their relative phases but also on their initial position separation. Lastly, interaction of an arbitrary number of vector solitons is also studied in brief. All our analytical results are supported by direct numerical simulations.

DOI: 10.1103/PhysRevE.64.026607 PACS number(s): 42.65.Tg, 05.45.Yv

I. INTRODUCTION

Optical fiber communications are advancing very rapidly both in lab experiments and in field installations nowadays. One of the major transmission formats is to use optical solitons as information bits. For each optical soliton, dispersion is balanced by fiber nonlinearity, thus the pulse can transmit without change of shape. However, when the bit rates are pushed very high, the tail interaction between adjacent pulses becomes non-negligible. This tail interaction causes a pulse to drift away from its expected position, a phenomenon called timing jitter in the optics literature. This timing jitter leads to signal detection error at the receiver end, and is detrimental to system performance. Motivated by its physical application, pulse-pulse interactions have been studied intensively in the past 20 years. Most of these studies used the nonlinear Schrödinger (NLS) equation model, which is appropriate when fiber birefringence is neglected. In such a case, it has been shown that when two equal-amplitude pulses are inphase (zero phase difference), they attract each other. When they are out-of-phase (π-phase difference), they repel each other. These results are confirmed experimentally in both optical fibers and photorefractive waveguides [1–3]. The interference between pulses can be reduced if pulses have different amplitudes (a quasistationary two-pulse bound state can be formed) [1,4,5], but it can never be eliminated, i.e., two pulses can never form a perfectly stationary bound state. In real optical fibers, birefringence is an intrinsic property and cannot be simply neglected. When fiber birefringence is taken into consideration, pulse propagation is actually governed by two coupled NLS equations [6]. In this case, each pulse generally consists of two polarization components that trap each other through nonlinear Kerr effects. Such a pulse is called a vector soliton in the optics literature. We note that a ''vector soliton'' here is just a solitary wave solution, not a soliton in the strict mathematical sense. A new phenomenon in the coupled NLS equations is that two vector solitons can form a perfectly stationary bound state if they have the same phase in one component and π-phase difference in the other component. Physically, stationary two-vector-soliton states can be formed because the attracting force in the in-phase polarization balances the repelling force in the out-of-phase polarization [7]. The existence of such stationary bound states was first established through numerical means by Haelterman *et al.* [7] (see also [8]). The analytical construction of such bound states was first achieved by Yang by an asymptotic tail-matching method [9]. In that work, the spacing between vector solitons in a stationary configuration was obtained explicitly. Similar results were reproduced later in Ref. [10] by dynamical system techniques. Experimentally, stationary two-vector-soliton states have been observed in photorefractive materials [11].

One important open question is the stability of stationary two-vector-soliton bound states. A more general question is the dynamics of interacting vector solitons. We note that the experimental observation of stationary two-vector-soliton states in Ref. [11] does not necessarily imply the stability of such states. The reason is that the propagation distance in that experiment was relatively short, thus weak instability would not have been detected. In Ref. [10], a special class of stationary two-vector-soliton bound states where each vector soliton has nearly 45° polarization was considered briefly. It was claimed that such states were linearly unstable, but that result was not substantiated. In the works [12,13], slightly different physical systems where the phase birefringence was weak or the nonlinearity was saturable were considered. In the former case, two-soliton bound states were found linearly unstable due to symmetry-breaking instability. In the latter case, linearly stable multihump solitons were discovered.

In this work, we study the interaction of two widely separated vector solitons that have nearly the same amplitudes, polarizations, and velocities. However, the common polarization of the two solitons is arbitrary (not restricted to 45° angles), so are the relative phases between them. As a special case, we will analytically reestablish the existence of stationary two-vector-soliton bound states and determine their stability properties. The method we will use is a modification of

*Email address: jyang@emba.uvm.edu

the Karpman-Solov'ev technique [14] (see also Gorshkov and Ostrovsky [15]). We first derive the dynamical equations for each vector-soliton's velocity, amplitude, position, and phase parameters. Then we show that these dynamical equations allow fixed points, which correspond to stationary two-vector-soliton bound states. There are two geometrically distinctive stationary bound states: one is that the larger-amplitude components of the two vector solitons are in phase, and the smaller-amplitude components are out-of-phase; the other one is that the larger-amplitude components are out-of-phase, and the smaller-amplitude components are in phase. These results reproduce those in Refs. [7–9], which were obtained differently. Next, we show that both these stationary bound states are linearly unstable. However, their instability characteristics are different. For the stationary bound state whose larger-amplitude components are in-phase, there are two unstable (purely real) eigenvalues, which are position- and phase related, respectively. But for the bound state whose larger-amplitude components are out-of-phase, there is only one unstable eigenvalue which is phase related. The position-related eigenvalues are now stable. Next, we discuss the full interaction dynamics of two vector solitons. We show that, in contrast to the single NLS equation, repulsion or attraction of two vector solitons depends not only on their phase differences, but also on their initial position separation. This can be understood intuitively by considering the attracting and repelling forces in vector solitons' two components. Lastly, we study the interaction of an arbitrary number of vector solitons. We present the dynamical equations for these solitons' internal parameters, and show that stationary bound states can be formed as well if neighboring solitons have the same phase in one component and π-phase difference in the other component, just like the two-vector-soliton case. But these bound states are also linearly unstable. All our analytical results are confirmed both qualitatively and quantitatively by the direct numerical simulations.

We emphasize that the modification of the Karpman and Solov'ev method as used in this paper does not depend on the integrability of the underlying wave equation. The key requirements are just that: (1) each individual pulse is linearly stable; (2) all pulses are nearly identical, moving at nearly the same velocities, and widely separated; and (3) the internal modes and radiation modes generated by tail-tail interactions are negligible. These requirements are satisfied in many integrable and nonintegrable equations in addition to the coupled NLS equations considered in this paper. Thus our generalized method can be widely applied for the study of pulse-pulse interactions.

The structure of this paper is arranged as follows. In Sec. II, we develop a one-vector-soliton perturbation theory, which is the foundation for the study of vector-soliton interactions. In Sec. III, we derive dynamical equations for internal parameters of two interacting vector solitons. In Sec. IV, we reestablish the existence of stationary two-vector-soliton bound states by examining the dynamical equations of interacting vector solitons. In Sec. V, we show that the stationary two-vector-soliton bound states are linearly unstable. In Sec. VI, we study the full interaction dynamics of two vector solitons and show that, with the same phase differences, two vector solitons can repel or attract each other for different initial position separations. In Sec. VII, we extend the results to an arbitrary number of vector solitons. Sec. VIII summarizes all the results, and makes some general comments related to our results.

II. ONE-VECTOR-SOLITON PERTURBATION THEORY

The coupled NLS equations are

$$iA_t + A_{xx} + (|A|^2 + \beta|B|^2)A = 0, \tag{2.1}$$

$$iB_t + B_{xx} + (|B|^2 + \beta|A|^2)B = 0, \tag{2.2}$$

where A and B are complex amplitudes of the electrical fields in the two orthogonal polarizations of an optical fiber, and β is the cross-phase modulational coefficient [6]. For linearly birefringent fibers, $\beta = 2/3$. If the birefringence is elliptic, β can take other values [16]. In a wavelength-division-multiplexed system, $\beta = 2$ (see [1,2]). If $\beta = 0$, the system becomes two decoupled NLS equations; if $\beta = 1$, it is called the Manakov model. In both cases, the system is integrable [17,18]. For other β values, it is nonintegrable. In this article, we allow β to be an arbitrary non-negative value except 1, i.e., we consider the general non-Manakov case.

Vector solitons of Eqs. (2.1) and (2.2) have the general form,

$$A = r(x - Vt - x_0)\exp\left[i\frac{V}{2}(x - Vt - x_0) + i\left(\omega^2 + \frac{V^2}{4}\right)t - i\gamma_0\right], \tag{2.3}$$

$$B = R(x - Vt - x_0)\exp\left[i\frac{V}{2}(x - Vt - x_0) + i\left(\Omega^2 + \frac{V^2}{4}\right)t - i\Gamma_0\right], \tag{2.4}$$

where ω and Ω are frequency parameters, V is the velocity, x_0 is the initial position, and γ_0 and Γ_0 are phase constants. Without loss, we take ω and Ω as positive numbers. Due to phase, position and Galilean invariances of Eqs. (2.1) and (2.2), the vector-soliton parameters V, x_0, γ_0 and Γ_0 are all arbitrary and can be normalized to be zero. But if one needs to study vector-soliton evolution under perturbations or vector-soliton interactions, all these parameters must be kept as variables as they will not be constants anymore (see later in this section and Sec. III). Amplitude functions $r(x)$ and $R(x)$ can be made entirely real due to phase invariances of Eqs. (2.1) and (2.2). Then these real amplitude functions satisfy the following ordinary differential equations (ODEs):

$$r_{xx} - \omega^2 r + (r^2 + \beta R^2)r = 0, \tag{2.5}$$

$$R_{xx} - \Omega^2 R + (R^2 + \beta r^2)R = 0. \tag{2.6}$$

Solutions to Eqs. (2.5) and (2.6) have been studied extensively before (see [8] and the references therein). It has been shown that for any frequency pair (ω,Ω) with Ω/ω lying inside the interval $([\sqrt{1+8\beta}-1]/2,\quad 2/[\sqrt{1+8\beta}-1])$ and $\beta\neq 1$, this ODE system has a unique single-hump vector-soliton solution that is symmetric in both r and R components. Thus we can use (ω,Ω) to characterize this unique single-hump solution. The asymptotic behavior of this solution at infinity is

$$r(x)\to ce^{-\omega|x|},\quad R(x)\to Ce^{-\Omega|x|},\quad |x|\to\infty, \tag{2.7}$$

where c and C are tail coefficients. When $\beta=1$, the interval $[(\sqrt{1+8\beta}-1)/2,\quad 2/(\sqrt{1+8\beta}-1)]$ shrinks to a single point 1. In this case, a single-hump vector soliton exists only when $\omega=\Omega$, but the polarization of this vector soliton is now arbitrary due to a rotational symmetry. Consequently, the parameters to characterize Manakov solitons are ω and polarization, rather than (ω,Ω). In this article, we study the interaction of single-hump vector solitons in non-Manakov systems. Thus we use (ω,Ω) to characterize each vector soliton during their interaction. Similar analysis can be done for the interaction of Manakov solitons, but the formulation needs a little modification. The ODE system (2.5) and (2.6) also supports many multihump vector-soliton solutions [8]. But we are not interested in the tail interaction of such vector solitons since evidence shows that they are all linearly unstable [8].

When two vector solitons are placed next to each other, they will interact due to tail overlapping. This pulse-pulse interaction has been studied intensively for the NLS equation and sine-Gordon equation, among others. The basic idea of Karpman and Solov'ev [14] (also Gorshkov and Ostrovsky [15]) is that, this tail overlapping acts as a small perturbation to each individual pulse. This perturbation causes each pulse to evolve adiabatically on a slow time scale. The radiation generated by the perturbation is small and negligible. In this article, we are going to use this idea to study vector soliton interactions. Since this idea critically depends on the perturbation theory for a single pulse, we will first develop this theory for a perturbed vector soliton in the remainder of this section.

Consider the perturbed coupled NLS equations

$$iA_t+A_{xx}+(|A|^2+\beta|B|^2)A=\epsilon F, \tag{2.8}$$

$$iB_t+B_{xx}+(|B|^2+\beta|A|^2)B=\epsilon G, \tag{2.9}$$

where functions F and G are perturbation terms, and ϵ is a small parameter. Without perturbations, the vector soliton (2.3) and (2.4) is an exact solution, and its internal parameters $\omega,\Omega,V,x_0,\gamma_0$, and Γ_0 are constants. When the perturbation is turned on, this vector soliton will evolve slowly on the time scale $T=\epsilon t$. The multiple-scale perturbation theory for this kind of evolution is well known (see [19], for instance). We write the perturbed solution as

$$A=\hat{r}(\theta,t,T)e^{iV\theta/2+i\gamma},\quad B=\hat{R}(\theta,t,T)e^{iV\theta/2+i\Gamma}, \tag{2.10}$$

where

$$\theta=x-\int_0^t V dt-x_0, \tag{2.11}$$

$$\gamma=\int_0^t(\omega^2+V^2/4)dt-\gamma_0,\quad \Gamma=\int_0^t(\Omega^2+V^2/4)dt-\Gamma_0. \tag{2.12}$$

Here velocity V, frequency parameters ω, Ω, initial position x_0, initial phases γ_0 and Γ_0 are all functions of slow time T. This slow time evolution can be determined when we pursue the perturbation theory to order ϵ. This will be done next.

We first substitute Eq. (2.10) into the evolution equations (2.8) and (2.9). Then equations for $\hat{r}$ and $\hat{R}$ are found to be

$$i\hat{r}_t+\hat{r}_{\theta\theta}-\omega^2\hat{r}+(|\hat{r}|^2+\beta|\hat{R}|^2)\hat{r} =\epsilon\overline{F}-\epsilon\left[i\hat{r}_T-ix_{0T}\hat{r}_\theta+\left(\frac{1}{2}Vx_{0T}-\frac{1}{2}V_T\theta+\gamma_{0T}\right)\hat{r}\right], \tag{2.13}$$

$$i\hat{R}_t+\hat{R}_{\theta\theta}-\Omega^2\hat{R}+(|\hat{R}|^2+\beta|\hat{r}|^2)\hat{R} =\epsilon\overline{G}-\epsilon\left[i\hat{R}_T-ix_{0T}\hat{R}_\theta+\left(\frac{1}{2}Vx_{0T}-\frac{1}{2}V_T\theta+\Gamma_{0T}\right)\hat{R}\right]. \tag{2.14}$$

Here

$$\overline{F}=Fe^{-iV\theta/2-i\gamma},\quad \overline{G}=Ge^{-iV\theta/2-i\Gamma}. \tag{2.15}$$

We now expand amplitude functions $\hat{r}$ and $\hat{R}$ into a perturbation series:

$$\hat{r}=r(\theta;\omega,\Omega)+\epsilon\tilde{r}+O(\epsilon^2), \tag{2.16}$$

$$\hat{R}=R(\theta;\omega,\Omega)+\epsilon\tilde{R}+O(\epsilon^2). \tag{2.17}$$

At the zeroth order, functions r and R just need to satisfy Eqs. (2.5) and (2.6), and we take them as a single-hump vector soliton. At order ϵ, equations for $\tilde{r}$ and $\tilde{R}$ can be written as

$$i\Psi_t+L\Psi=W. \tag{2.18}$$

Here

$$L=\begin{pmatrix} \partial_{\theta\theta}-\omega^2+2r^2+\beta R^2 & r^2 & \beta rR & \beta rR \\ -r^2 & -\partial_{\theta\theta}+\omega^2-2r^2-\beta R^2 & -\beta rR & -\beta rR \\ \beta rR & \beta rR & \partial_{\theta\theta}-\Omega^2+2R^2+\beta r^2 & R^2 \\ -\beta rR & -\beta rR & -R^2 & -\partial_{\theta\theta}+\Omega^2-2R^2-\beta r^2 \end{pmatrix}, \quad (2.19)$$

$$\Psi=(\tilde{r},\tilde{r}^*,\tilde{R},\tilde{R}^*)^T, \quad (2.20)$$

$$W=(W_1,-W_1^*,W_2,-W_2^*)^T, \quad (2.21)$$

the superscript "T" represents the matrix transpose, the superscript "*" represents the complex conjugate,

$$W_1=\overline{F}_0-\left[ir_T-ix_{0T}r_\theta+\left(\frac{1}{2}Vx_{0T}-\frac{1}{2}V_T\theta+\gamma_{0T}\right)r\right], \quad (2.22)$$

$$W_2=\overline{G}_0-\left[iR_T-ix_{0T}R_\theta+\left(\frac{1}{2}Vx_{0T}-\frac{1}{2}V_T\theta+\Gamma_{0T}\right)R\right], \quad (2.23)$$

and functions $\overline{F}_0$ and $\overline{G}_0$ are just $\overline{F}$ and $\overline{G}$ evaluated at $A=r(\theta)e^{iV\theta/2+i\gamma}$ and $B=R(\theta)e^{iV\theta/2+i\Gamma}$. In order for the perturbation theory to hold, functions $\overline{F}_0$ and $\overline{G}_0$ must be slowly varying with time.

Operator L has three discrete eigenstates with zero eigenvalue:

$$\Psi_1=(r,-r,0,0)^T, \quad (2.24)$$

$$\Psi_2=(0,0,R,-R)^T, \quad (2.25)$$

$$\Psi_3=(r_\theta,r_\theta,R_\theta,R_\theta)^T. \quad (2.26)$$

These eigenstates are related to the phase and position invariances of the vector soliton solution (2.3) and (2.4). Operator L also has three generalized eigenstates for the zero eigenvalue:

$$\Phi_1=(r_\omega,r_\omega,R_\omega,R_\omega)^T, \quad (2.27)$$

$$\Phi_2=(r_\Omega,r_\Omega,R_\Omega,R_\Omega)^T, \quad (2.28)$$

$$\Phi_3=(\theta r,-\theta r,\theta R,-\theta R)^T. \quad (2.29)$$

These generalized states are related to amplitude and velocity variations of the vector soliton (2.3) and (2.4). In addition,

$$L\Phi_1=2\omega\Psi_1, \quad L\Phi_2=2\Omega\Psi_2, \quad L\Phi_3=2\Psi_3. \quad (2.30)$$

In order for the inhomogeneous solution Ψ of the first-order equation (2.18) to be non-secular at large time, the inhomogeneous term in Eq. (2.18) must be orthogonal to the above eigenstates and generalized eigenstates of eigenvalue zero, i.e.,

$$\langle W,\Psi_k\rangle=\langle W,\Phi_k\rangle=0, \quad k=1,2,3. \quad (2.31)$$

Here the inner product is defined as

$$\langle f,g\rangle=\int_{-\infty}^{\infty}f^T\,\mathrm{diag}(1,-1,1,-1)g\,d\theta, \quad (2.32)$$

where "diag (.)" represents a diagonal matrix with diagonal elements inside the parentheses. Evaluating the above six integrals in Eq. (2.31), the slow-time evolution equations for $x_0,\gamma_0,\Gamma_0,V,\omega$ and Ω will be obtained. Defining masses of the unperturbed vector-soliton's two components as

$$M(\omega,\Omega)=\int_{-\infty}^{\infty}r^2(\theta;\omega,\Omega)d\theta,$$

$$N(\omega,\Omega)=\int_{-\infty}^{\infty}R^2(\theta;\omega,\Omega)d\theta, \quad (2.33)$$

these evolution equations can be written as

$$\frac{dM}{dT}=2\int_{-\infty}^{\infty}r\,\mathrm{Im}(\overline{F}_0)d\theta, \quad (2.34)$$

$$\frac{dN}{dT}=2\int_{-\infty}^{\infty}R\,\mathrm{Im}(\overline{G}_0)d\theta, \quad (2.35)$$

$$(M+N)\frac{dV}{dT}=4\int_{-\infty}^{\infty}\mathrm{Re}(r_\theta\overline{F}_0+R_\theta\overline{G}_0)d\theta, \quad (2.36)$$

$$(M+N)_\omega V\frac{dx_0}{dT}+2M_\omega\frac{d\gamma_0}{dT}+2N_\omega\frac{d\Gamma_0}{dT}=4\int_{-\infty}^{\infty}\mathrm{Re}(r_\omega\overline{F}_0+R_\omega\overline{G}_0)d\theta, \quad (2.37)$$

$$(M+N)_\Omega V\frac{dx_0}{dT}+2M_\Omega\frac{d\gamma_0}{dT}+2N_\Omega\frac{d\Gamma_0}{dT}=4\int_{-\infty}^{\infty}\mathrm{Re}(r_\Omega\overline{F}_0+R_\Omega\overline{G}_0)d\theta, \quad (2.38)$$

$$(M+N)\frac{dx_0}{dT}=2\int_{-\infty}^{\infty}\mathrm{Im}(\theta r\overline{F}_0+\theta R\overline{G}_0)d\theta. \quad (2.39)$$

Here "Re" and "Im" represent the real and imaginary parts of a complex number. These six equations are the main re-

sults of the single-vector-soliton perturbation theory. They will be critical for the development of vector-soliton interaction theory in the next section. We note that in the above analysis, we have focused on the evolution of the vector-soliton itself under perturbations. We have not paid any attention to the radiation that is generated by the perturbation, nor have we considered the internal modes of operator L that can also be excited by perturbations (the existence of internal modes for vector solitons has been extensively studied in [20,21]). This is legitimate for weak perturbations, as radiation and internal modes in that case are indeed small and negligible.

III. VECTOR-SOLITON INTERACTIONS

In this section, we study the interaction of two vector solitons that have nearly the same amplitudes, polarizations and velocities, and are separated far apart. Here the tail overlapping can be considered as a small perturbation, which causes each vector soliton to evolve on a slow time scale ϵt. Here ϵ is the magnitude of tail overlapping, which is exponentially small with soliton spacing. For convenience, we will not introduce ϵ explicitly in the analysis below. But we do need to distinguish between fast variables and slow variables as in Sec. II.

As the leading order approximation, the solution is a superposition of two widely separated vector solitons:

$$A=A_1+A_2, \quad B=B_1+B_2, \tag{3.1}$$

where

$$A_k=r_k(\theta_k,t)\exp[iV_k\theta_k/2+i\gamma_k],$$
$$B_k=R_k(\theta_k,t)\exp[iV_k\theta_k/2+i\Gamma_k], \tag{3.2}$$

$$\theta_k=x-x_k, \quad x_k=\int_0^t V_k dt+x_{k0}, \tag{3.3}$$

$$\gamma_k=\int_0^t(\omega_k^2+V_k^2/4)dt-\gamma_{k0}, \quad \Gamma_k=\int_0^t(\Omega_k^2+V_k^2/4)dt-\Gamma_{k0}. \tag{3.4}$$

For the convenience of description, we put the first pulse on the left side, and the second pulse on the right side, i.e., $x_1<x_2$. Now we substitute Eq. (3.1) into the original system (2.1) and (2.2). Since the two solitons are widely separated, collecting terms that are the dominating contribution to the evolution of each pulse, we can split Eqs. (2.1) and (2.2) into two systems, one for each pulse:

$$iA_{kt}+A_{kxx}+(|A_k|^2+\beta|B_k|^2)A_k=F_k, \tag{3.5}$$

$$iB_{kt}+B_{kxx}+(|B_k|^2+\beta|A_k|^2)B_k=G_k, \tag{3.6}$$

where

$$F_k=-2|A_k|^2A_{3-k}-A_k^2A_{3-k}^*-\beta(A_kB_kB_{3-k}^*+A_kB_k^*B_{3-k}+|B_k|^2A_{3-k}), \tag{3.7}$$

$$G_k=-2|B_k|^2B_{3-k}-B_k^2B_{3-k}^*-\beta(B_kA_kA_{3-k}^*+B_kA_k^*A_{3-k}+|A_k|^2B_{3-k}), \tag{3.8}$$

and $k=1,2$. Note that terms F_k and G_k are due to tail overlapping of the two vector solitons. These terms now act as perturbations on each vector soliton, as Eqs. (3.5) and (3.6) indicate. This idea has been mentioned before in this article.

To proceed further, we need to recall our assumptions, which are that the two vector solitons have nearly the same amplitudes, polarizations and velocities, and are separated far apart. With the notations

$$\omega\equiv(\omega_2+\omega_1)/2, \quad \Omega\equiv(\Omega_2+\Omega_1)/2, \quad V\equiv(V_2+V_1)/2, \tag{3.9}$$

$$\Delta\omega\equiv\omega_2-\omega_1, \quad \Delta\Omega\equiv\Omega_2-\Omega_1, \quad \Delta V\equiv V_2-V_1, \tag{3.10}$$

and

$$\Delta\gamma\equiv\gamma_2-\gamma_1, \quad \Delta\Gamma\equiv\Gamma_2-\Gamma_1, \quad \Delta x\equiv x_2-x_1, \tag{3.11}$$

these assumptions are simply

$$|\Delta\omega|\ll\omega, \quad |\Delta\Omega|\ll\Omega, \quad |\Delta V|\ll|V|, \quad \omega\Delta x\gg1,$$
$$\Omega\Delta x\gg1, \quad |\Delta\omega\Delta x|\ll1, \quad |\Delta\Omega\Delta x|\ll1. \tag{3.12}$$

Since $|\Delta V|\ll|V|$, we get

$$(V_2\theta_2-V_1\theta_1)/2\approx-V\Delta x/2. \tag{3.13}$$

Then applying the single vector-soliton perturbation theory of Sec. II to Eqs. (3.5) and (3.6), we obtain the dynamical equations for each vector-soliton's internal parameters as

$$\frac{dM_k}{dt}=2(-1)^{k+1}\int_{-\infty}^{\infty}r_k(r_k^2+\beta R_k^2)r_{3-k}dx \times\sin(V\Delta x/2-\Delta\gamma), \tag{3.14}$$

$$\frac{dN_k}{dt}=2(-1)^{k+1}\int_{-\infty}^{\infty}R_k(R_k^2+\beta r_k^2)R_{3-k}dx \times\sin(V\Delta x/2-\Delta\Gamma), \tag{3.15}$$

$$(M_k+N_k)\frac{dV_k}{dt}=4\int_{-\infty}^{\infty}r_k(r_k^2+\beta R_k^2)r_{3-k,x}dx \times\cos(V\Delta x/2-\Delta\gamma) +4\int_{-\infty}^{\infty}R_k(R_k^2+\beta r_k^2)R_{3-k,x}dx \times\cos(V\Delta x/2-\Delta\Gamma), \tag{3.16}$$

$$(M_k+N_k)_{\omega_k}V_k\frac{dx_{k0}}{dt}+2M_{k,\omega_k}\frac{d\gamma_{k0}}{dt}+2N_{k,\omega_k}\frac{d\Gamma_{k0}}{dt}$$
$$=-4\int_{-\infty}^{\infty}[r_k(r_k^2+\beta R_k^2)]_{\omega_k}r_{3-k}dx\cos(V\Delta x/2-\Delta\gamma)$$
$$-4\int_{-\infty}^{\infty}[R_k(R_k^2+\beta r_k^2)]_{\omega_k}R_{3-k}dx\cos(V\Delta x/2-\Delta\Gamma), \tag{3.17}$$

$$(M_k+N_k)_{\Omega_k}V_k\frac{dx_{k0}}{dt}+2M_{k,\Omega_k}\frac{d\gamma_{k0}}{dt}+2N_{k,\Omega_k}\frac{d\Gamma_{k0}}{dt}$$
$$=-4\int_{-\infty}^{\infty}[r_k(r_k^2+\beta R_k^2)]_{\Omega_k}r_{3-k}dx\cos(V\Delta x/2-\Delta\gamma)$$
$$-4\int_{-\infty}^{\infty}[R_k(R_k^2+\beta r_k^2)]_{\Omega_k}R_{3-k}dx\cos(V\Delta x/2-\Delta\Gamma), \tag{3.18}$$

$$(M_k+N_k)\frac{dx_{k0}}{dt}$$
$$=2(-1)^{k+1}\int_{-\infty}^{\infty}(x-x_k)r_k(r_k^2+\beta R_k^2)r_{3-k}dx$$
$$\times\sin(V\Delta x/2-\Delta\gamma)+2(-1)^{k+1}\int_{-\infty}^{\infty}(x-x_k)R_k$$
$$\times(R_k^2+\beta r_k^2)R_{3-k}dx\sin(V\Delta x/2-\Delta\Gamma). \tag{3.19}$$

Here $k=1$ and 2. The above dynamical equations can be simplified greatly. First, recall that r_k and R_k satisfy the ordinary differential equations (2.5) and (2.6). In addition, the tail behavior of the vector soliton with averaged frequencies (ω,Ω) is given by Eq. (2.7). Then, in view of the assumptions (3.12), the integrals in Eqs. (3.14), (3.15), and (3.16) can be calculated explicitly (to the leading order). For instance,

$$\int_{-\infty}^{\infty}r_1(r_1^2+\beta R_1^2)r_2dx=\int_{-\infty}^{\infty}(\omega^2r-r_{xx})ce^{\omega(x-\Delta x)}dx$$
$$=ce^{-\omega\Delta x}[\omega re^{\omega x}-r_xe^{\omega x}]_{-\infty}^{\infty}$$
$$=2\omega c^2e^{-\omega\Delta x}. \tag{3.20}$$

In this calculation, integration by parts has been carried out. Similarly, we can show that

$$\int_{-\infty}^{\infty}r_k(r_k^2+\beta R_k^2)r_{3-k}dx=2\omega c^2e^{-\omega\Delta x}, \tag{3.21}$$

$$\int_{-\infty}^{\infty}R_k(R_k^2+\beta r_k^2)R_{3-k}dx=2\Omega C^2e^{-\Omega\Delta x}, \tag{3.22}$$

$$\int_{-\infty}^{\infty}r_k(r_k^2+\beta R_k^2)r_{3-k,x}dx=(-1)^{k+1}2\omega^2c^2e^{-\omega\Delta x}, \tag{3.23}$$

and

$$\int_{-\infty}^{\infty}R_k(R_k^2+\beta r_k^2)R_{3-k,x}dx=(-1)^{k+1}2\Omega^2C^2e^{-\Omega\Delta x}. \tag{3.24}$$

Further simplification of Eqs. (3.14), (3.15), and (3.16) can be achieved if we derive dynamical equations for parameter differences $\Delta\omega$, $\Delta\Omega$, and ΔV instead of these parameters themselves. For this purpose, we notice from Eqs. (3.14) and (3.21) that, to leading order,

$$(M_1+M_2)_t=0, \tag{3.25}$$

$$(M_2-M_1)_t=-8\omega c^2e^{-\omega\Delta x}\sin(V\Delta x/2-\Delta\gamma). \tag{3.26}$$

Then, since

$$M_{kt}=M_\omega(\omega_k,\Omega_k)\omega_{kt}+M_\Omega(\omega_k,\Omega_k)\Omega_{kt},\quad k=1,2, \tag{3.27}$$

and

$$\omega_k=\omega+(-1)^k\Delta\omega/2,\quad \Omega_k=\Omega+(-1)^k\Delta\Omega/2,\quad k=1,2, \tag{3.28}$$

Eqs. (3.25) and (3.26) become

$$M_\omega\omega_t+M_\Omega\Omega_t=0, \tag{3.29}$$

and

$$M_\omega\Delta\omega_t+M_\Omega\Delta\Omega_t=-8\omega c^2e^{-\omega\Delta x}\sin(V\Delta x/2-\Delta\gamma). \tag{3.30}$$

Here partial derivatives M_ω and M_Ω are evaluated at averaged frequencies (ω,Ω). Similar calculations show that

$$N_\omega\omega_t+N_\Omega\Omega_t=0, \tag{3.31}$$

$$N_\omega\Delta\omega_t+N_\Omega\Delta\Omega_t=-8\Omega C^2e^{-\Omega\Delta x}\sin(V\Delta x/2-\Delta\Gamma), \tag{3.32}$$

$$V_t=0, \tag{3.33}$$

and

$$(M+N)\Delta V_t=-16[\omega^2c^2e^{-\omega\Delta x}\cos(V\Delta x/2-\Delta\gamma)$$
$$+\Omega^2C^2e^{-\Omega\Delta x}\cos(V\Delta x/2-\Delta\Gamma)]. \tag{3.34}$$

We note that Eqs. (3.29) and (3.31) are equivalent to

$$\omega_t=\Omega_t=0. \tag{3.35}$$

To simplify Eqs. (3.17), (3.18), and (3.19), we notice that the two vector solitons are nearly identical [see assumptions (3.12)]. Thus, to leading order, the right-hand sides of Eqs.

(3.17), (3.18) and (3.19) are the same for $k=1$ and 2. From Eqs. (3.3) and (3.4), we see that

$$x_{k0t}=x_{kt}-V_k, \quad \gamma_{k0t}=\omega_k^2+\frac{1}{4}V_k^2-\gamma_{kt},$$

$$\Gamma_{k0t}=\Omega_k^2+\frac{1}{4}V_k^2-\Gamma_{kt}. \tag{3.36}$$

We also know that

$$V_k=V+(-1)^k\Delta V/2. \tag{3.37}$$

Then equating the left-hand sides of Eqs. (3.17), (3.18), and (3.19) for $k=1$ and 2, these equations simplify to

$$\frac{d\Delta x}{dt}=\Delta V, \tag{3.38}$$

$$\frac{d\Delta\gamma}{dt}=\frac{1}{2}V\Delta V+2\omega\Delta\omega, \tag{3.39}$$

and

$$\frac{d\Delta\Gamma}{dt}=\frac{1}{2}V\Delta V+2\Omega\Delta\Omega. \tag{3.40}$$

Now, we summarize the evolution equations for vector-soliton parameters after the above simplifications. If we introduce two new notations:

$$\Delta\phi=-\frac{1}{2}V\Delta x+\Delta\gamma, \quad \Delta\Phi=-\frac{1}{2}V\Delta x+\Delta\Gamma, \tag{3.41}$$

the final evolution equations can be deduced from Eqs. (3.29) to (3.40) as follows:

$$\omega_t=\Omega_t=V_t=0, \tag{3.42}$$

$$\begin{bmatrix} M_\omega & M_\Omega \\ N_\omega & N_\Omega \end{bmatrix}\begin{bmatrix} \Delta\omega_t \\ \Delta\Omega_t \end{bmatrix}=\begin{bmatrix} 8\omega c^2 e^{-\omega\Delta x}\sin\Delta\phi \\ 8\Omega C^2 e^{-\Omega\Delta x}\sin\Delta\Phi \end{bmatrix}, \tag{3.43}$$

$$(M+N)\Delta V_t=-16(\omega^2c^2e^{-\omega\Delta x}\cos\Delta\phi + \Omega^2C^2e^{-\Omega\Delta x}\cos\Delta\Phi), \tag{3.44}$$

$$\Delta x_t=\Delta V, \tag{3.45}$$

$$\Delta\phi_t=2\omega\Delta\omega, \tag{3.46}$$

$$\Delta\Phi_t=2\Omega\Delta\Omega. \tag{3.47}$$

We remind the reader that $M(\omega,\Omega)$ and $N(\omega,\Omega)$ are a vector soliton's two component masses defined in Eq. (2.33), and c and C are tail coefficients of a vector soliton defined in Eq. (2.7).

Dynamical equations (3.42) to (3.47) are the main results of this paper. They completely determine the evolution of two vector solitons under tail interactions. Equation (3.42) indicates that the averaged frequencies (or equivalently, amplitude and polarization) and velocity of the two vector solitons remain unchanged during this interaction. The parameter differences are governed by Eqs. (3.43) to (3.47).

When $\beta=0$, system (2.1) and (2.2) becomes two decoupled NLS equations. Therefore, the dynamical equations (3.42) to (3.47) should reproduce those for the single NLS equation as a special case. This is true indeed. We note that when $\beta=0$,

$$r(x)=\sqrt{2}\omega\,\mathrm{sech}\,\omega x, \quad R(x)=\sqrt{2}\Omega\,\mathrm{sech}\,\Omega x. \tag{3.48}$$

Thus

$$M=4\omega, \quad N=4\Omega, \tag{3.49}$$

and

$$c=2\sqrt{2}\omega, \quad C=2\sqrt{2}\Omega. \tag{3.50}$$

When these relations are substituted into dynamical equations (3.42) to (3.47), we find that those equations can be split into two independent sets of equations. Each set of equations governs the evolution of a NLS soliton, and they are precisely the ones derived by Karpman and Solov'ev [14] and Gorshkov and Ostrovsky [15] (see also [1]). Thus our results reproduce the previous ones as a special case. But our results are much more general, applying to any cross-phase coupling coefficient $\beta\neq1$. When $\beta=1$ (Manakov case), vector solitons are characterized by ω and the polarization angle instead of ω and Ω. In that case, the dynamical equations need to be formulated a little differently. This could be easily done, but we will leave it elsewhere.

One important fact about the dynamical equations (3.42) to (3.47) is that they allow a simple reduction. It proves to be consistent if we ask that

$$\Delta\omega=\Delta\Omega=0, \quad \Delta\phi=0 \text{ or } \pi, \quad \Delta\Phi=0 \text{ or } \pi. \tag{3.51}$$

Then, those equations reduce to a single second-order equation for the vector-soliton separation Δx:

$$(M+N)\Delta x_{tt}+16[\omega^2c^2e^{-\omega\Delta x}\cos\Delta\phi + \Omega^2C^2e^{-\Omega\Delta x}\cos\Delta\Phi]=0. \tag{3.52}$$

We note that similar reduction exists for the single NLS equation as well. Equation (3.52) may allow fixed points when $\cos\Delta\phi$ and $\cos\Delta\Phi$ are of opposite sign. This fixed point then gives the spacing for a stationary two-vector-soliton bound state. This issue will be examined in greater detail in the next section.

IV. EXISTENCE OF STATIONARY TWO-VECTOR-SOLITON BOUND STATES

With the dynamical equations (3.42) to (3.47) now available, one can proceed to study interaction dynamics for various initial conditions, as has been done extensively for the NLS equation (see [1] and the references therein). However, in this and the next sections, we take a different path and study the formation of stationary two-vector-soliton bound states and their linear stability. The existence of these station-

ary bound states holds only for the coupled NLS equations, not for the single NLS equation. This existence has been established before both numerically and analytically (see [7–9]). But the stability problem has not been resolved yet. In this section, we rederive stationary two-vector-soliton bound states by virtue of the dynamical equations (3.42) to (3.47). Stability issue will be considered in the next section.

Stationary two-vector-soliton bound states in the coupled NLS system (2.1) and (2.2) simply correspond to fixed points of the dynamical equations (3.43) to (3.47). There are two fixed points in these dynamical equations:

$$\text{(I)}\ \Delta\omega=\Delta\Omega=\Delta V=0,\quad \Delta\phi=\pi,\quad \Delta\Phi=0, \tag{4.1}$$

$$\text{(II)}\ \Delta\omega=\Delta\Omega=\Delta V=0,\quad \Delta\phi=0,\quad \Delta\Phi=\pi. \tag{4.2}$$

In the first case, the A components of the two vector solitons are out-of-phase (π-phase difference), and the B components are in phase (zero phase difference). In other words, the A components are antisymmetric, and the B components are symmetric. In the second case, the situation is just the opposite, i.e., the A components are symmetric, and the B components are antisymmetric. In both cases, the spacing Δx_* is found from Eq. (3.52) as

$$\Delta x_*=\frac{\ln\Omega^2C^2-\ln\omega^2c^2}{\Omega-\omega}. \tag{4.3}$$

Of course, the spacing obtained from this formula has to be such that $\Delta x_*\gg 1$, an assumption we have made throughout the paper. A fact we have found is that only when $0<\beta<1$ can positive spacing Δx_* be obtained from formula (4.3). When $\beta\to 1^-$, spacings from this formula approach infinity for every (ω,Ω) pair where a single-hump vector soliton is allowed. Thus stationary two-vector-soliton bound states do not exist in the Manakov model ($\beta=1$). We note, however, that other stationary bound states not of two-vector-soliton type do exist in the Manakov model (see [22]). When $\beta>1$, Δx_* from formula (4.3) is negative, thus no stationary state of two well-separated vector solitons is predicted from our analysis above. However, numerical results in [7,8] show that such stationary states still exist for $\beta>1$ when $\Omega\approx\omega$. This dilemma needs to be resolved in the future. Below when we discuss stationary bound states, we take $0<\beta<1$, so that our analysis gives the correct prediction. Note that formula (4.3) was first obtained by this author using an entirely different technique, namely, the asymptotic tail-matching method [9]. That method and its results were very general (not restricted to the coupled NLS equations). But it could not be used to study the stability problem. These same results were later reproduced in Ref. [10] by dynamical systems techniques. But the stability issue was barely touched there. The current perturbation method, however, could establish the existence of stationary two-vector-soliton bound states and resolve their stability issue completely (see later in this section and the next section).

The existence of stationary two-vector-soliton bound states is a phenomenon which is absent in the single NLS equation. An intuitive explanation for this existence has been given in [7] in terms of force balances as follows. It is well known that in the single NLS equation, if two solitons are in phase, they attract each other. But if they are out-of-phase, they repel each other. Vector solitons in the coupled NLS equations have two components (A and B). If solitons are in phase in one component, but out-of-phase in the other component, then a stationary bound state can be formed if the attracting force in the in-phase component exactly balances the repelling force in the out-of-phase component. This is exactly what happens in the two types of stationary bound states (4.1) and (4.2). We note that this force balance occurs only at a specific position separation Δx_* which is given in Eq. (4.3). At other position separations, the forces will not be in balance, thus the two solitons will move relative to each other (see Sec. VI).

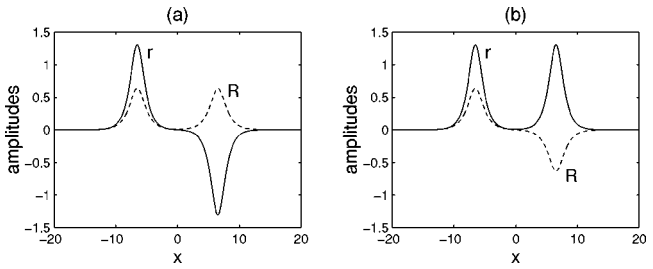

FIG. 1. Numerically obtained stationary two-vector-soliton bound states for $\beta=2/3$, $\omega=1$, and $\Omega=0.85$ (solid: r; dashed: R). (a) Type I state with r antisymmetric and R symmetric; (b) type II state with r symmetric and R antisymmetric. Analytical approximations by Eqs. (4.1), (4.2), and (4.3) are indistinguishable from the numerical curves and thus not shown.

Next, we compare the above analytical results on stationary two-vector-soliton bound states with numerical results. We choose the following parameter values: $\beta=2/3$ and $\omega=1$. Then for each Ω lying inside the interval $(0.7583,1.3187)$, there is a unique single-hump vector soliton solution. The tail coefficients c and C of single-hump vector solitons can be easily determined numerically by shooting techniques. Our analysis above predicts two types of stationary two-vector-soliton bound states in Eqs. (2.5) and (2.6): type I has r antisymmetric, and R symmetric; type II has r symmetric, and R antisymmetric. The analytically predicted spacings Δx_* are given by formula (4.3). To confirm these analytical results, we have numerically determined multihump solitary waves in Eqs. (2.5) and (2.6) by shooting techniques (see also [7,8]). Sure enough, we numerically found both types of stationary two-vector-soliton bound states. These states with $\Omega=0.85$ are shown in Fig. 1 for illustration. The numerical spacings of these two bound states, measured as the distance between the two highest $|r|$ points in the graph, are 13.0622 and 13.0644, respectively. For this Ω value, tail coefficients of the single-hump vector soliton are found as $c=2.6592$ and $C=1.1744$. Thus, the analytical spacing from formula (4.3) is 13.0635 for both bound states. The analytical spacing agrees very well with the numerical spacings. If we plot the analytical approximations for the two-vector-soliton bound states, which are superpositions of two single-hump vector solitons with 0 or π phase differences and separated apart at spacing Δx_*

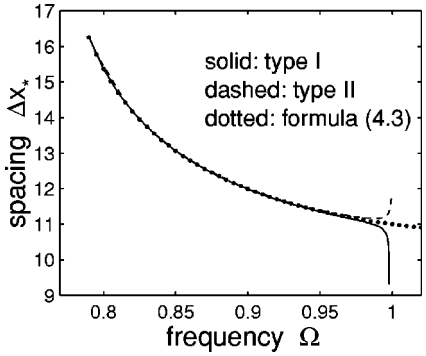

FIG. 2. Spacings of type I and II two-vector-soliton bound states for $\beta=2/3$, $\omega=1$, and various Ω values. Solid curve, type I spacing (numerical); dashed curve, type II spacing (numerical); dotted curve, analytical formula (4.3).

$=13.0635$, the analytical curves and exact numerical ones are indistinguishable. Thus the analytical curves are not shown in Fig. 1.

Further comparison between the exact (numerical) soliton spacing in a stationary two-vector-soliton state and the analytical formula (4.3) can be made when we vary Ω continuously. This is done in Fig. 2, where we plot the numerical spacings for type I and II bound states and the analytical spacing (4.3) simultaneously. As we can see, when Ω is not close to 1, the agreement between numerics and theory is very good. As Ω approaches 1, the numerical results diverge from the analytical prediction. Specifically, as Ω approaches 1, type I spacing plummets, while type II spacing rises to infinity. One interesting question is that, while type II spacing goes to infinity as Ω approaches 1, why cannot the perturbation theory formula (4.3) predict it? The reason may lie in the fact that the perturbation theory predicts the same spacing for both type I and II bound states, while the actual spacings for the two bound states go different ways when Ω approaches 1. But this question needs further investigation.

V. LINEAR STABILITY OF STATIONARY TWO-VECTOR-SOLITON BOUND STATES

In this section, we analytically determine the linear stability of type I and II bound states (4.1) and (4.2) [see Fig. 1]. This will be done by examining the linear stability of fixed points (4.1) and (4.2) in the ODE system (3.43) to (3.47). We first consider the fixed point I. When this point is perturbed, we can write

$$\Delta\omega=\Delta\tilde{\omega},\quad \Delta\Omega=\Delta\tilde{\Omega},\quad \Delta V=\Delta\tilde{V}, \tag{5.1}$$

$$\Delta\phi=\pi+\Delta\tilde{\phi},\quad \Delta\Phi=\Delta\tilde{\Phi},\quad \Delta x=\Delta x_*+\Delta\tilde{x}, \tag{5.2}$$

where the tilded quantities are small perturbations. Substituting these perturbed quantities into the dynamical equations (3.43) to (3.47) and neglecting higher-order terms, we get

$$\begin{bmatrix}\Delta\tilde{\phi}\\ \Delta\tilde{\Phi}\end{bmatrix}_{tt}=\frac{1}{M_\omega N_\Omega-M_\Omega N_\omega}\begin{bmatrix}-16\omega^2c^2N_\Omega e^{-\omega\Delta x_*} & -16\omega\Omega C^2M_\Omega e^{-\Omega\Delta x_*}\\ 16\omega\Omega c^2N_\omega e^{-\omega\Delta x_*} & 16\Omega^2C^2M_\omega e^{-\Omega\Delta x_*}\end{bmatrix}\begin{bmatrix}\Delta\tilde{\phi}\\ \Delta\tilde{\Phi}\end{bmatrix}, \tag{5.3}$$

and

$$\Delta\tilde{x}_{tt}-\frac{16(\omega-\Omega)\omega^2c^2}{M+N}e^{-\omega\Delta x_*}\Delta\tilde{x}=0. \tag{5.4}$$

Notice that the above equations for the phase and position perturbations are decoupled. Now we put the perturbed quantities in the normal-mode form:

$$\Delta\tilde{\phi}=\alpha_1e^{\lambda t},\quad \Delta\tilde{\Phi}=\alpha_2e^{\lambda t},\quad \Delta\tilde{x}=\alpha_3e^{\lambda t}, \tag{5.5}$$

where λ is the discrete eigenvalue. When this form is substituted into Eq. (5.4), position-related eigenvalues λ_{po} are found as

$$\lambda_{po}^2=\frac{16(\Omega-\omega)\omega^2c^2}{M+N}e^{-\omega\Delta x_*}. \tag{5.6}$$

There are two such eigenvalues, $\pm\lambda_{po}$, where λ_{po} is a root of the right-hand-side quantity in Eq. (5.6). Notice that λ_{po} is either purely real, or purely imaginary, depending on the sign of $\omega-\Omega$. When $\omega>\Omega$, it is purely imaginary, thus is stable. If $\omega<\Omega$, λ_{po} is purely real, thus unstable.

When Eq. (5.5) is substituted into Eq. (5.3), phase-related eigenvalues λ_{ph} are found to satisfy the fourth-order polynomial equation

$$\lambda_{ph}^4+\frac{16\omega^2c^2(N_\Omega-M_\omega)}{M_\omega N_\Omega-M_\Omega N_\omega}e^{-\omega\Delta x_*}\lambda_{ph}^2-\frac{16^2\omega^2\Omega^2c^2C^2}{M_\omega N_\Omega-M_\Omega N_\omega}e^{-(\omega+\Omega)\Delta x_*}=0. \tag{5.7}$$

The roots of this equation are $\pm\lambda_{ph}^{(1)}$ and $\pm\lambda_{ph}^{(2)}$, where

$$\lambda_{ph}^{(1)2}\lambda_{ph}^{(2)2}=-\frac{16^2\omega^2\Omega^2c^2C^2}{M_\omega N_\Omega-M_\Omega N_\omega}e^{-(\omega+\Omega)\Delta x_*}. \tag{5.8}$$

To determine the stability of these phase-related eigenvalues, it is necessary to obtain the sign of the determinant $M_\omega N_\Omega-M_\Omega N_\omega$. For this purpose, we normalize the solutions (r,R) in Eqs. (2.5) and (2.6) as

$$r(x;\omega,\Omega)=\omega\overline{r}(\overline{x};p), \tag{5.9}$$

$$R(x;\omega,\Omega)=\omega\overline{R}(\overline{x};p), \tag{5.10}$$

where

$$\overline{x}=\omega x, \quad p=\Omega^2/\omega^2, \tag{5.11}$$

and the normalized solutions $\overline{r}(\overline{x};p)$ and $\overline{R}(\overline{x};p)$ satisfy the new ODEs:

$$\overline{r}_{\overline{x}\overline{x}}-\overline{r}+(\overline{r}^2+\beta\overline{R}^2)\overline{r}=0, \tag{5.12}$$

$$\overline{R}_{\overline{x}\overline{x}}-p\overline{R}+(\overline{R}^2+\beta\overline{r}^2)\overline{R}=0. \tag{5.13}$$

With the further mass notations

$$\overline{M}(p)=\int_{-\infty}^{\infty}\overline{r}^2(\overline{x};p)d\overline{x}, \quad \overline{N}(p)=\int_{-\infty}^{\infty}\overline{R}^2(\overline{x};p)d\overline{x}, \tag{5.14}$$

we see that

$$M(\omega,\Omega)=\omega\overline{M}(p), \quad N(\omega,\Omega)=\omega\overline{N}(p). \tag{5.15}$$

With these relations, we readily find that the determinant is given by

$$M_\omega N_\Omega-M_\Omega N_\omega=2\sqrt{p}\overline{M}^2(p)\frac{d}{dp}\left[\frac{\overline{N}(p)}{\overline{M}(p)}\right]. \tag{5.16}$$

When $0\leqslant\beta<1$ where meaningful stationary two-vector-soliton bound states exist, $\overline{N}(p)/\overline{M}(p)$ is an increasing function of p. This can be understood heuristically as follows. For the ODE system (5.12) and (5.13), single-hump vector solitons exist when p lies in the interval $([\sqrt{1+8\beta}-1]/2,\ 2/[\sqrt{1+8\beta}-1])$ (see Sec. II). If $0\leqslant\beta<1$, $[\sqrt{1+8\beta}-1]/2<1<2/[\sqrt{1+8\beta}-1]$, thus $[\sqrt{1+8\beta}-1]/2$ is the lower bound, and $2/[\sqrt{1+8\beta}-1]$ is the upper bound. When p is close to the lower bound, the vector soliton is a wave and daughter-wave structure where $\overline{R}(x)\ll\overline{r}(x)$, thus $\overline{N}/\overline{M}$ is very small (see [8]). As p increases, function $R(x)$ becomes larger relative to $r(x)$, thus $\overline{N}/\overline{M}$ also increases. When $p=1$, we have $R(x)=r(x)$, so $\overline{N}/\overline{M}=1$. As p increases further, $R(x)$ becomes larger, and $r(x)$ becomes smaller. When p is close to its upper bound, the vector soliton is again a wave and daughter-wave structure, but now $\overline{r}(x)\ll\overline{R}(x)$, thus $\overline{N}/\overline{M}\gg1$. We see that as p steadily increases from its lower bound to its upper bound, so does $\overline{N}/\overline{M}$, consequently $\overline{N}/\overline{M}$ is an increasing function of p. Of course, we have verified this fact numerically as well.

Since $\overline{N}/\overline{M}$ is an increasing function of p, the determinant (5.16) is positive. It is then clear from Eq. (5.8) that one of $\lambda_{ph}^{(1)2}$ and $\lambda_{ph}^{(2)2}$ is positive, and the other one is negative. Without loss, we denote $\lambda_{ph}^{(1)2}$ as positive, and $\lambda_{ph}^{(2)2}$ negative. Then eigenvalues $\pm\lambda_{ph}^{(1)}$ are purely real, and $\pm\lambda_{ph}^{(2)}$ purely imaginary. Of the two purely real eigenvalues $\pm\lambda_{ph}^{(1)}$, one of them is positive and thus unstable. The imaginary eigenvalues $\pm\lambda_{ph}^{(2)}$ are stable.

Similar stability analysis can be done for the other fixed point II [see Eq. (4.2)]. We can readily show that the six eigenvalues for fixed point II are exactly

$$\pm i\lambda_{po}, \quad \pm i\lambda_{ph}^{(1)}, \quad \pm i\lambda_{ph}^{(2)}, \tag{5.17}$$

where λ_{po}, $\lambda_{ph}^{(1)}$ and $\lambda_{ph}^{(2)}$ are given by Eqs. (5.6) and (5.7). This means that $\pm i\lambda_{ph}^{(1)}$ are now stable eigenvalues since $i\lambda_{ph}^{(1)}$ is imaginary, and one of $\pm i\lambda_{ph}^{(2)}$ is unstable since $i\lambda_{ph}^{(2)}$ is now real. The position-related eigenvalues $\pm i\lambda_{po}$ are stable or unstable depending on whether $\pm\lambda_{po}$ for fixed point I are unstable or stable. Specifically, when $\omega<\Omega$, $i\lambda_{po}$ is real, thus one of $\pm i\lambda_{po}$ is positive and unstable. When $\omega>\Omega$, both $\pm i\lambda_{po}$ are imaginary and stable. We note that for $0\leqslant\beta<1$, the r component in the single-hump vector soliton is larger than the R component when $\omega>\Omega$, and smaller when $\omega<\Omega$. Thus, for both type I and II stationary bound states, when the larger-amplitude component changes sign (π-phase difference), the position-related eigenvalues are stable. When the larger-amplitude component does not change sign (same phase), one of the position-related eigenvalues becomes unstable. Whether the larger-amplitude component changes sign or not, exactly one phase-related eigenvalue is always unstable.

Our stability results obtained above can be summarized as follows. Both type I and II stationary bound states are linearly unstable because there is always one (and only one) phase-related eigenvalue that is unstable. When the larger-amplitude component does not change sign, there is one position-related eigenvalue that is unstable as well. Otherwise, position-related eigenvalues are stable.

Below we compare the above analytically obtained eigenvalues for stationary bound states with numerical results. Numerically, we determined the discrete nonzero eigenvalues and corresponding eigenfunctions of the linearization operator expanded around the underlying stationary bound state, again using the shooting method. We note that for this linearization operator, it is easy to show that if λ is an eigenvalue, so are $-\lambda$ and λ^*. Thus, when λ is purely real or imaginary, it leads to a pair of eigenvalues. When λ is truly complex, it leads to four eigenvalues. Numerically, we only look for discrete eigenvalues that are close to zero, as the eigenvalues we have obtained analytically above are of this type. Altogether, we found exactly six such discrete eigenvalues, all of them either purely real or purely imaginary. Thus they always come in pairs with opposite signs. This agrees perfectly with the analysis. In addition, two of these six eigenfunctions roughly have the shape of spatial derivatives of two single-hump vector solitons pieced together. Their eigenvalues correspond to the position-related eigenvalues $\pm\lambda_{po}$ or $\pm i\lambda_{po}$ discussed above. The other four eigenfunctions roughly have the shape of two single-hump vector solitons joined together. Their eigenvalues correspond to phase-related eigenvalues $\pm\lambda_{ph}^{(1)}$ and $\pm\lambda_{ph}^{(2)}$ (or $\pm i\lambda_{ph}^{(1)}$ and $\pm i\lambda_{ph}^{(2)}$). To make a quantitative comparison, we choose $\beta=2/3$, $\omega=1$, and allow Ω to take various values.

The numerically obtained eigenvalues and the corresponding analytical eigenvalues are plotted in Figs. 3 and 4 for bound states I and II, respectively. Note that for each

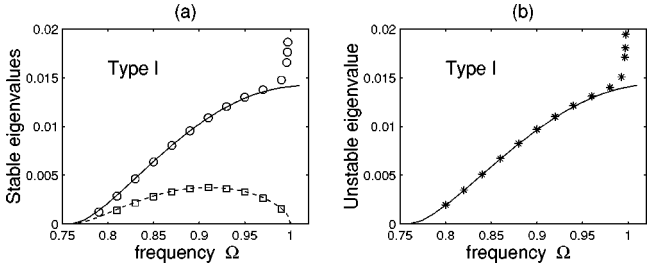

FIG. 3. Discrete eigenvalues for type I stationary two-vector-soliton bound states with $\beta=2/3$, $\omega=1$ and various Ω values. (a) Stable eigenvalues, o, phase related, obtained numerically; □, position related, obtained numerically; solid curve, $|\lambda_{ph}^{(2)}|$ from formula (5.7); dashed curve: $|\lambda_{po}|$ from formula (5.6); (b) unstable eigenvalue, *, phase related, obtained numerically; solid curve, $|\lambda_{ph}^{(1)}|$ from formula (5.7).

case, only three of the six eigenvalues are shown, as the other three are simply their opposites. We also note that the two solid analytical curves in Fig. 3(a,b) and Fig. 4(a,b) for $|\lambda_{ph}^{(2)}|$ and $|\lambda_{ph}^{(1)}|$, respectively, are slightly different, even though they look alike. Let us consider Fig. 3 for bound states I first. We see in this figure that when $\Omega<1$, there is indeed an unstable phase-related eigenvalue that is the counterpart of $\lambda_{ph}^{(1)}$ in the analysis above. The other phase-related eigenvalue ($\lambda_{ph}^{(2)}$) and position-related eigenvalue (λ_{po}) are both stable. This agrees with the theory. Quantitative comparisons between numerical and analytical eigenvalues are excellent except when Ω approaches 1. The reason for the disagreement when Ω is close to 1 is simple. Recall from Fig. 2 that as Ω approaches 1, the spacing for type I bound states drops steeply. Thus our basic assumption of far separation between the two vector solitons breaks down, consequently disagreement is not unexpected. Interestingly, this disagreement is only in the phase-related eigenvalues, not in the position-related eigenvalue. In Fig. 3(b), the numerically obtained unstable eigenvalue rises sharply as Ω approaches 1. This is understandable since the two solitons get closer and closer, thus a stronger instability is created.

Next we consider Fig. 4 for bound states II. In this case, numerical results show that a phase-related eigenvalue (counterpart of $i\lambda_{ph}^{(2)}$) and the position-related eigenvalue (counterpart of $i\lambda_{po}$) are both unstable, and the other phase-related eigenvalue ($i\lambda_{ph}^{(1)}$) is stable. This agrees with our analysis. As in Fig. 3, numerical and analytical eigenvalues agree very well except when Ω is close to 1. Numerically, the two phase-related eigenvalues drop to zero as $\Omega\rightarrow 1^{-}$. The reason is also simple. For type II bound states, soliton spacing approaches infinity as $\Omega\rightarrow 1^{-}$ (see Fig. 2). Thus the bound state becomes two separate single vector solitons. Naturally the phase-related eigenvalues (as well as the position-related eigenvalue) collapse to the zero eigenvalue of a single vector soliton.

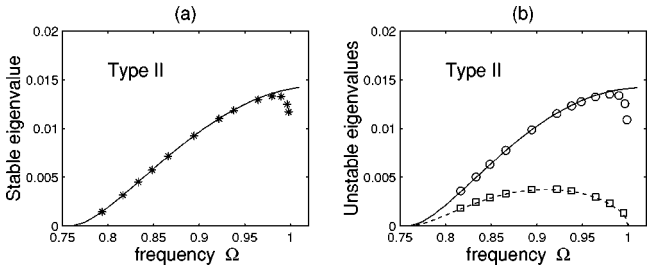

FIG. 4. Discrete eigenvalues for type II stationary two-vector-soliton bound states with $\beta=2/3$, $\omega=1$, and various Ω values. (a) Stable eigenvalue. *, phase related, obtained numerically; solid curve: $|\lambda_{ph}^{(1)}|$ from formula (5.7). (b) Unstable eigenvalues. o, phase related, obtained numerically; □, position related, obtained numerically; solid curve, $|\lambda_{ph}^{(2)}|$ from formula (5.7); dashed curve, $|\lambda_{po}|$ from formula (5.6).

Now, we put our results in the eigenvalue bifurcation perspective. When $0<\beta<1$, the linearization operator around one single-hump vector soliton has six or eight discrete eigenvalues (multiplicity counted), depending on whether an internal mode exists or not (see Refs. [20,21]). The zero eigenvalue always has multiplicity 6, three from position and phase invariances, and the other three from velocity and frequency (or amplitude) variations. When an internal mode exists, two purely imaginary eigenvalues of opposite sign are present as well. If two vector solitons form a stationary bound state, the linearization operator around this state will have 12 or 16 discrete eigenvalues (double that for a single vector soliton). Now the zero eigenvalue still has multiplicity 6. Another six eigenvalues must bifurcate from the zero eigenvalue, and another four must bifurcate from the two internal-mode eigenvalues when such modes do exist. Our calculations above give exactly the six eigenvalues bifurcated from the zero eigenvalue. These six eigenvalues are the most important as they are related to the dynamics of vector solitons themselves. Our analysis did not give eigenvalues bifurcated from internal modes (if such modes do exist). The reason is that to obtain those eigenvalues, one has to pursue the perturbation theory to second order (see Ref. [19]). Since the six nonzero eigenvalues we have obtained already reveal the linear instability of these bound states, we do not have a strong motivation to pursue eigenvalues bifurcated from internal modes. Similarly, it is also possible for eigenvalues to bifurcate from the edge of the continuous spectrum in a stationary two-vector-soliton bound state. But our instability results make such calculations not compelling either.

VI. INTERACTION DYNAMICS

In this section, we study interaction dynamics of two vector solitons. In particular, we will highlight the interaction dynamics of vector solitons, namely, repulsion or attraction of vector solitons depends not only on the relative phases but also on the initial position separation. To restrict the scope of our discussion, we will consider only the interaction of two vector solitons that initially have the same amplitude, polarization and velocity, but their relative phases are allowed to differ by 0 or π, and their initial separation is allowed to be arbitrary. In such cases, the initial conditions can be written as

$$A(x,0)=r\left(x+\frac{\Delta x_0}{2}\right)+r\left(x-\frac{\Delta x_0}{2}\right)e^{i\gamma_0}, \qquad (6.1)$$

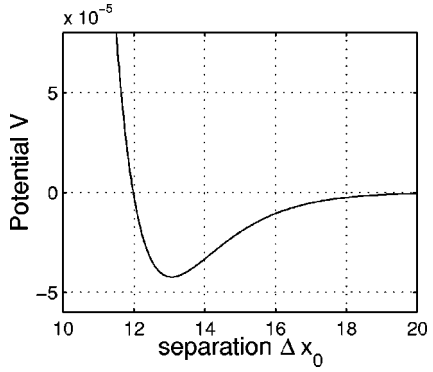

FIG. 5. Interaction potential (6.4) of two vector solitons with $\gamma_0=\pi$, $\Gamma_0=0$, $\beta=2/3$, $\omega=1$, and $\Omega=0.85$ for various position separations Δx_0.

$$B(x,0)=R\left(x+\frac{\Delta x_0}{2}\right)+R\left(x-\frac{\Delta x_0}{2}\right)e^{i\Gamma_0}. \tag{6.2}$$

Here $[r(x),R(x)]$ is a single-hump vector soliton, Δx_0 is the initial position separation, and γ_0,Γ_0 are initial phase differences which are either 0 or π. For demonstration purpose, we also take the following parameters values $\beta=2/3$, $\omega=1$ and $\Omega=0.85$. The single-hump vector soliton for these parameters look like one half of either Fig. 1(a) or Fig. 1(b).

For the initial conditions chosen above, the reduction (3.51) holds. Thus our theory in Sec. III predicts that this soliton interaction is governed by the second-order equation (3.52) on pulse separation Δx. This equation can be rewritten as

$$(M+N)\Delta x_{tt}+V'(\Delta x)=0, \tag{6.3}$$

where the potential function $V(\Delta x)$ is

$$V(\Delta x)=-16\cos\gamma_0 c^2\omega e^{-\omega\Delta x}-16\cos\Gamma_0 C^2\Omega e^{-\Omega\Delta x}. \tag{6.4}$$

For the chosen parameters, it is found numerically that $(c,C)=(2.6592,1.1744)$ and $(M,N)=(3.4459,0.9080)$. Different from the single NLS equation where the interaction potential is always monotone [1], potential (6.4) now can have a local maximum or minimum when $\cos\gamma_0\cos\Gamma_0<0$. This is why in such cases a stationary two-vector-soliton bound state can be found. For our choice of parameters, when $\gamma_0=\pi$ and $\Gamma_0=0$, this potential is shown in Fig. 5. We see that it has a local minimum (which is also its global minimum) at $\Delta x_*=13.0635$, and this minimum point is stable. For any initial separation $\Delta x_0>11.9804$, the motion is trapped inside the potential well, thus two vector solitons will oscillate around this stable minimum point. But if $\Delta x_0<11.9804$, the initial potential energy would be too large so that the two vector solitons would simply separate infinitely apart from each other. This qualitative change in interaction dynamics for different initial pulse separations is a feature that is not present in the single NLS equation. If $\gamma_0=0$ and $\Gamma_0=\pi$, the potential is exactly opposite of that in Fig. 5 (a vertical reflection about the horizontal axis). Thus it has a global maximum at $\Delta x_*=13.0635$. This maximum point is unstable. When $\Delta x_0>13.0635$, two solitons repel each other; when $\Delta x_0<13.0635$, they attract each other and collapse.

The interaction dynamics for $(\gamma_0,\Gamma_0)=(0,0)$ and $(\gamma_0,\Gamma_0)=(\pi,\pi)$ can be determined similarly from the potential function. For $(\gamma_0,\Gamma_0)=(0,0)$, the potential is monotone increasing. Thus with any initial separation, two vector solitons attract each other and collapse. When $(\gamma_0,\Gamma_0)=(\pi,\pi)$, the situation is just the opposite. Now the potential is monotone decreasing. Thus two solitons always repel each other. Interaction dynamics in these two cases is quite similar to that in a single NLS equation.

The above interaction dynamics can be understood intuitively in terms of attractive and repulsive force balances in vector-solitons' individual components. It is well known that in the single NLS equation, if two solitons are in phase (zero phase difference), an attracting force exists between them; if the solitons are out-of-phase (π phase difference), a repelling force exists between them. The magnitude of the attracting or repelling force is proportional to the integral of product of tail amplitudes in the overlapping region. For vector solitons, the same picture holds. However, since vector solitons have two components, the combined force of the two components will determine if vector solitons attract or repel each other. When soliton separation changes, so does the amount of interaction force in each component, thus the amount of combined force overall. But it is important to realize that a change in soliton separation causes different amounts of change in interaction forces of the two components, as soliton amplitudes $r(x)$ and $R(x)$ decay at rates ω and Ω, which are different if ω and Ω are different [see Eq. (2.7)]. This is the fundamental reason why repulsion or attraction of vector solitons depends not only on their relative phases but also on their initial separation. To be more specific, let us analyze the interaction (6.1) and (6.2) for $\gamma_0=0$ and $\Gamma_0=\pi$ for instance. The other parameters β,ω and Ω are as chosen above, i.e., 2/3,1 and 0.85, respectively. We have established in Sec. IV that when $\Delta x_0=\Delta x_*=13.0635$, two vector solitons form a stationary bound state because the attracting and repelling forces in the two components exactly balance each other. Now if the initial soliton separation is greater than Δx_*, the attractive force in the *A* component decreases more than the repulsive force in the *B* component. As a result, the force balance is broken, and the net force between the two vector solitons becomes repulsive. Thus solitons will move away from each other. On the other hand, if the initial separation is smaller than Δx_*, the attractive force in the *A* component increases more than the repulsive force in the *B* component. Thus the net force becomes attractive, and solitons will move toward each other. These intuitive expectations agree entirely with the analyses above. Other cases can be understood in a similar way.

We would like to remind the reader that the reduction (6.3) when γ_0 and Γ_0 are 0 or π ignores phase instabilities in the full dynamical equations (3.43) to (3.47). In fact, the minimum point Δx_* in the potential (6.4) is stable only to position perturbations, but not to phase perturbations, since we have proved in Sec. V that stationary two-vector-soliton bound states are always subject to phase-related instabilities. When initial phase perturbations are small, and the interac-

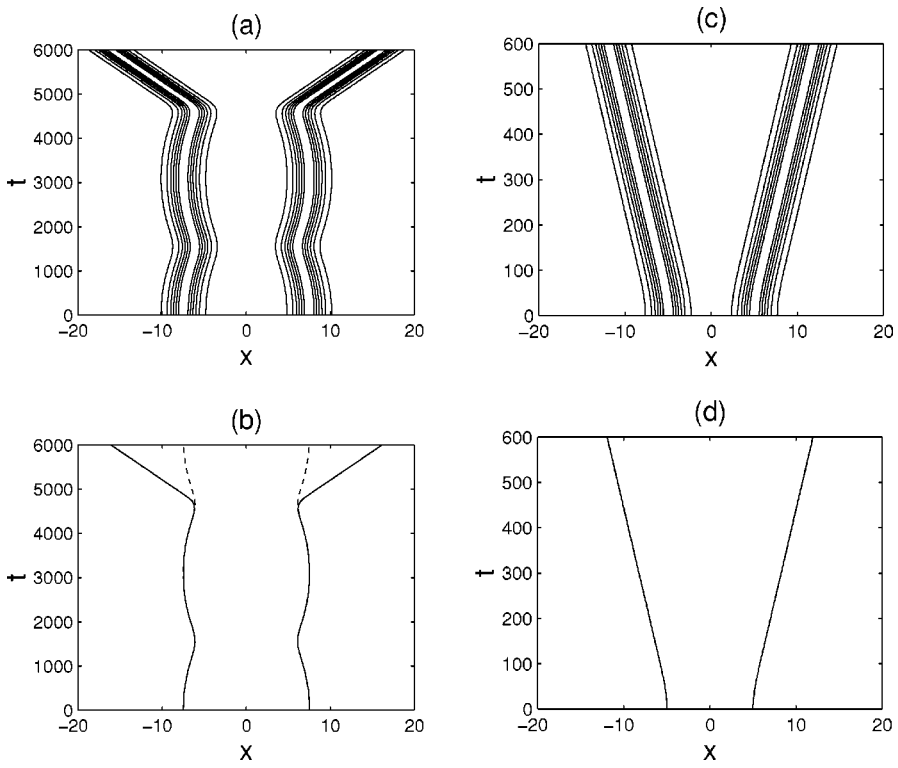

FIG. 6. Interaction dynamics of two vector solitons with $\gamma_0 = \pi$, $\Gamma_0 = 0$, $\Delta x_0 = 15$ or 10 in the initial condition (6.1) and (6.2). Here $\beta = 2/3$, $\omega = 1$, and $\Omega = 0.85$. (a) $\Delta x_0 = 15$: $|A|$ contour, obtained numerically ($|B|$ contour is similar); (b) $\Delta x_0 = 15$: positions of vector solitons. Solid curve: numerical results; dashed curve: analytical prediction from Eq. (6.3); (c) $\Delta x_0 = 10$: $|A|$ contour, obtained numerically; (d) $\Delta x_0 = 10$: positions of vector solitons. Solid curve: numerical results; dashed curve: analytical prediction from Eq. (6.3). Here the two curves overlap completely with each other.

tion time is not very long, phase instabilities are mild. In that case, the reduced model (6.3) will describe vector-soliton interactions very well. But if phase perturbations have accumulated to a significant amount, model (6.3) will break down.

All the above analytical and intuitive predictions on vector-soliton interactions are completely supported both qualitatively and quantitatively by our full numerical simulations of Eqs. (2.1) and (2.2), using Eqs. (6.1) and (6.2) as the initial condition. First we take $(\gamma_0, \Gamma_0) = (\pi, 0)$ and $\Delta x_0 = 15$. The numerical results are shown in Fig. 6(a). Here only $|A|$ contour is shown, as $|B|$ contour is similar. As predicted, the two solitons engage in oscillational motions around spacing $\Delta x_* = 13.0635$. In Fig. 6(b), we plot in solid lines the positions of both vector solitons (defined as locations of maximum $|A|$ amplitudes) against time. In the same figure, positions of vector solitons obtained from the reduced model (6.3) are also shown for comparison. The numerical and analytical curves completely overlap with each other until $t \gtrsim 4600$. The reason for deviation after $t \gtrsim 4600$ is simply the development of phase instabilities which we have mentioned above. This phase instability was ignored in the reduced model (6.3). But in the numerical solution, numerical error triggers this instability and causes the relative phases in the A and B components to move away from their initial values π and 0. This change in relative phases eventually leads to the repulsion of solitons as seen in Fig. 6(a). Next, we still take $(\gamma_0, \Gamma_0) = (\pi, 0)$ but choose the initial separation $\Delta x_0 = 10$. In this case, our analysis above predicts that the two vector solitons would repel each other. This is confirmed by our numerical solutions shown in Fig. 6(c). A comparison between the numerical vector-soliton positions and analytical predictions by the reduced model (6.3) is shown in Fig. 6(d). In this case, the two curves completely overlap each other for all times.

Next, we take other γ_0, Γ_0, and Δx_0 values, and show in Fig. 7 vector-soliton interactions that are obtained numerically. Here the interaction's dependence on initial separation as well as relative phases will be demonstrated, and similarities with interactions in a single NLS equation will be highlighted. In each case, numerical results and the analysis based on the reduced model (6.3) agree completely when the two solitons are well separated. Thus analytical results will not be shown. In Fig. 7(a), we took $(\gamma_0, \Gamma_0) = (0, \pi)$, $\Delta x_0 = 15$, and found that the solitons repel each other and escape. In Fig. 7b, we took $(\gamma_0, \Gamma_0) = (0, \pi)$, $\Delta x_0 = 10$, and found that the solitons attract each other and collapse. After collapse, the two solitons reemerge and separate. In Fig. 7c, $(\gamma_0, \Gamma_0) = (0, 0)$ and $\Delta x_0 = 10$ were taken. The solitons attract each other and collapse. But here, after collapse, the two solitons merge into one instead of reemerging and separating. In Fig. 7d, $(\gamma_0, \Gamma_0) = (\pi, \pi)$ and $\Delta x_0 = 10$ were taken. The solitons repel each other and escape. Interaction dynamics in Figs. 6 and 7(a,b) shows that vector-soliton interactions depend critically on the initial position separation as well as on relative phases. Interaction dynamics in Fig. 7(c,d) resembles that in a single NLS equation, as the relative phases in the A and B components here are of the same value, thus repelling or attracting forces in the two components combine instead of canceling each other.

More studies on interaction of vector solitons are needed. For instance, one can take as initial conditions two vector solitons with different amplitudes, or phase differences other than 0 and π. In such cases, one would need to investigate the full ODE model (3.43) to (3.47) instead of the reduced one (6.3). But these studies lie outside the scope of the present paper.

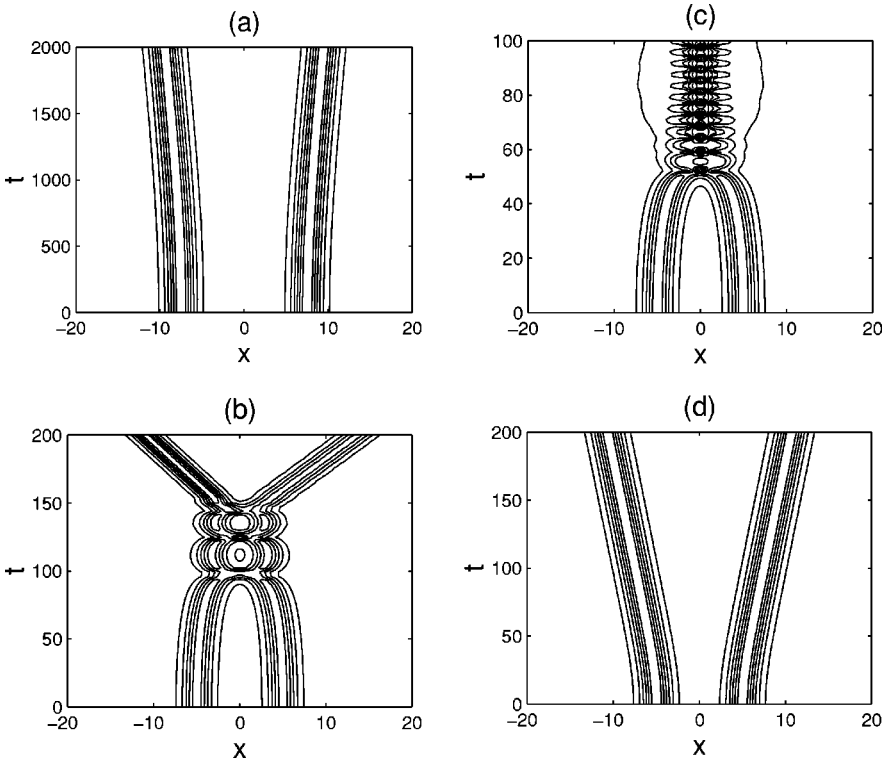

FIG. 7. Interaction dynamics of two vector solitons for various γ_0, Γ_0, and Δx_0 values in the initial condition (6.1) and (6.2). Shown are numerically obtained $|A|$ contours. Here $\beta=2/3$, $\omega=1$ and $\Omega=0.85$. (a) $\gamma_0=0$, $\Gamma_0=\pi$, $\Delta x_0=15$; (b) $\gamma_0=0$, $\Gamma_0=\pi$, $\Delta x_0=10$; (c) $\gamma_0=0$, $\Gamma_0=0$, $\Delta x_0=10$; (d) $\gamma_0=\pi$, $\Gamma_0=\pi$, $\Delta x_0=10$.

VII. INTERACTION OF *N* VECTOR SOLITONS

Lastly, we briefly discuss the interaction of three or more vector solitons. Such interactions can be investigated by extending our two-soliton interaction results. Suppose we have N vector solitons with frequencies (ω_k, Ω_k), velocities V_k, positions x_k, and phases (γ_k, Γ_k), where $1\leqslant k\leqslant N$. Define averaged variables

$$\omega=\frac{1}{N}\sum_{k=1}^{N}\omega_k, \quad \Omega=\frac{1}{N}\sum_{k=1}^{N}\Omega_k, \quad V=\frac{1}{N}\sum_{k=1}^{N}V_k, \tag{7.1}$$

and difference variables

$$\Delta\omega_k=\omega_{k+1}-\omega_k, \quad \Delta\Omega_k=\Omega_{k+1}-\Omega_k,$$

$$\Delta V_k=V_{k+1}-V_k, \tag{7.2}$$

$$\Delta\gamma_k=\gamma_{k+1}-\gamma_k, \quad \Delta\Gamma_k=\Gamma_{k+1}-\Gamma_k, \quad \Delta x_k=x_{k+1}-x_k, \tag{7.3}$$

$$\Delta\phi_k=-\frac{1}{2}V\Delta x_k+\Delta\gamma_k, \quad \Delta\Phi_k=-\frac{1}{2}V\Delta x_k+\Delta\Gamma_k, \tag{7.4}$$

where $1\leqslant k\leqslant N-1$. Then under the adiabatic assumptions similar to Eq. (3.12), we readily derive the following evolution equations for the N vector solitons:

$$\omega_t=\Omega_t=V_t=0, \tag{7.5}$$

$$\begin{aligned}M_\omega\Delta\omega_{kt}+M_\Omega\Delta\Omega_{kt}=4\omega c^2[&-e^{-\omega\Delta x_{k-1}}\sin\Delta\phi_{k-1}\\&+2e^{-\omega\Delta x_k}\sin\Delta\phi_k\\&-e^{-\omega\Delta x_{k+1}}\sin\Delta\phi_{k+1}],\end{aligned} \tag{7.6}$$

$$\begin{aligned}N_\omega\Delta\omega_{kt}+N_\Omega\Delta\Omega_{kt}=4\Omega C^2[&-e^{-\Omega\Delta x_{k-1}}\sin\Delta\Phi_{k-1}\\&+2e^{-\Omega\Delta x_k}\sin\Delta\Phi_k\\&-e^{-\Omega\Delta x_{k+1}}\sin\Delta\Phi_{k+1}],\end{aligned} \tag{7.7}$$

$$\begin{aligned}(M+N)\Delta V_{kt}=&8[\omega^2c^2e^{-\omega\Delta x_{k-1}}\cos\Delta\phi_{k-1}\\&+\Omega^2C^2e^{-\Omega\Delta x_{k-1}}\cos\Delta\Phi_{k-1}]\\&-16[\omega^2c^2e^{-\omega\Delta x_k}\cos\Delta\phi_k\\&+\Omega^2C^2e^{-\Omega\Delta x_k}\cos\Delta\Phi_k]\\&+8[\omega^2c^2e^{-\omega\Delta x_{k+1}}\cos\Delta\phi_{k+1}\\&+\Omega^2C^2e^{-\Omega\Delta x_{k+1}}\cos\Delta\Phi_{k+1}],\end{aligned} \tag{7.8}$$

$$\Delta x_{kt}=\Delta V_k, \tag{7.9}$$

$$\Delta\phi_{kt}=2\omega\Delta\omega_k, \tag{7.10}$$

$$\Delta\Phi_{kt}=2\Omega\Delta\Omega_k, \tag{7.11}$$

where $1\leqslant k\leqslant N-1$. Component masses $M(\omega,\Omega)$ and $N(\omega,\Omega)$ are defined in Eq. (2.33), tail coefficients c and C are defined in Eq. (2.7), and conventions

$$e^{-\omega\Delta x_0}=e^{-\Omega\Delta x_0}=e^{-\omega\Delta x_N}=e^{-\Omega\Delta x_N}=0 \tag{7.12}$$

have been used. Similar to the two-vector-soliton case, dynamical equations (7.6) to (7.11) also allow the reduction

$$\Delta\omega_k=\Delta\Omega_k=0,\quad \Delta\phi_k=0 \text{ or } \pi,\quad \Delta\Phi_k=0 \text{ or } \pi,$$
$$1\leqslant k\leqslant N-1. \tag{7.13}$$

Then those equations reduce to

$$\begin{aligned}(M+N)\Delta x_{ktt}=&8[\omega^2c^2e^{-\omega\Delta x_{k-1}}\cos\Delta\phi_{k-1}\\&+\Omega^2C^2e^{-\Omega\Delta x_{k-1}}\cos\Delta\Phi_{k-1}]\\&-16[\omega^2c^2e^{-\omega\Delta x_k}\cos\Delta\phi_k\\&+\Omega^2C^2e^{-\Omega\Delta x_k}\cos\Delta\Phi_k]\\&+8[\omega^2c^2e^{-\omega\Delta x_{k+1}}\cos\Delta\phi_{k+1}\\&+\Omega^2C^2e^{-\Omega\Delta x_{k+1}}\cos\Delta\Phi_{k+1}].\end{aligned} \tag{7.14}$$

This reduced equation [as well as the full dynamical equations (7.6) to (7.11)] allows fixed points where

$$\cos\Delta\phi_k\cos\Delta\Phi_k=-1, \tag{7.15}$$

and

$$\Delta x_k=\Delta x_*=\frac{\ln\Omega^2C^2-\ln\omega^2c^2}{\Omega-\omega} \tag{7.16}$$

for $1\leqslant k\leqslant N-1$. These fixed points correspond to stationary N-vector-soliton bound states. Eq. (7.15) indicates that in these bound states, neighboring vector solitons must have the same phase in one component (same sign), and π-phase difference in the other component (opposite sign), just as the two-vector-soliton case. We note that these N-vector-soliton bound states have been constructed before in Ref. [9] by an asymptotic tail matching technique. The matching conditions and soliton spacing given in Ref. [9] are the same as above. Linear stability of these stationary bound states can be determined by examining the stability of fixed points (7.13), (7.15), and (7.16) in the evolution equations (7.6) to (7.11). Not surprisingly, we find these states to be always linearly unstable due to phase instabilities. Interaction dynamics of multiple vector solitons is richer than that of two vector solitons. One interesting example is shown in Fig. 8 for a three-vector-soliton interaction. The parameter values are still $\beta=2/3$, $\omega=1$ and $\Omega=0.85$. The initial condition is

$$A(x,0)=r(x-x_l)e^{i\gamma_{l0}}+r(x)+r(x-x_r)e^{i\gamma_{r0}}, \tag{7.17}$$

$$B(x,0)=R(x-x_l)e^{i\Gamma_{l0}}+R(x)+R(x-x_r)e^{i\Gamma_{r0}}, \tag{7.18}$$

where (r,R) is the single-hump vector soliton, $x_l=-11$, $x_r=15$, $\gamma_{l0}=0$, $\gamma_{r0}=\pi$, $\Gamma_{l0}=\pi$, and $\Gamma_{r0}=0$. We see that in the initial stage, the interaction of these solitons can still be understood by considering them as pair-pair interactions. But after collapse of the left two solitons, our perturbation analysis completely fails. Beyond that point, we see more interesting interaction dynamics.

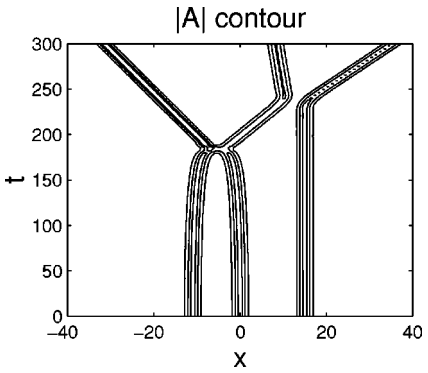

FIG. 8. An interesting interaction dynamics of three vector solitons. Shown here is the $|A|$ contour. The initial condition is Eqs. (7.17) and (7.18), where $\beta=2/3$, $\omega=1$, $\Omega=2/3$, $x_l=-11$, $x_r=15$, $\gamma_{l0}=0$, $\gamma_{r0}=\pi$, $\Gamma_{l0}=\pi$, and $\Gamma_{r0}=0$.

VIII. DISCUSSIONS

In summary, we have studied the interaction of two vector solitons in the coupled NLS equations (non-Manakov). Under the assumption that the two vector solitons have nearly the same amplitudes, polarizations, velocities, and are separated far apart, we derived the dynamical equations for both solitons' internal parameters. These equations reveal the existence of stationary two-vector-soliton bound states when one of the vector-soliton's two components changes sign. But these bound states are shown to be linearly unstable due to a phase-related unstable eigenvalue. Study of the interaction shows that, in contrast to the single NLS equation, vector solitons repel or attract each other depending not only on the relative phases but also on the initial position separation. This fact was explained heuristically by considering force balances in vector solitons' two components. We also presented dynamical equations for the interaction of an arbitrary number of vector solitons. We showed that these solitons can also form stationary bound states, but these states are linearly unstable as well.

One question about the dynamical equations (3.43) to (3.47), or (7.6) to (7.11) in general, is whether they can be cast as a complex Toda system (coupled to another equation perhaps since we have six equations here). For the single NLS case, this was possible by defining the complex variable as a combination of position separation and phase difference (see Refs. [15,23]). Inspection of Eqs. (3.43) to (3.47) suggests that in the present case, this is not possible for $\beta\neq0$ or 1 (nonintegrable case). The reason is that in order for a complex Toda system to exist, coefficients in the dynamical equations must satisfy certain compatibility conditions. These conditions are not likely to be satisfied by Eqs. (3.43) to (3.47), or (7.6) to (7.11). This claim is consistent with the results for generalized NLS equations where the complex Toda chain reduction was found only for the integrable NLS equation [24]. It is likely that the Manakov model $\beta=1$ can allow such reductions. But our dynamical equations do not

apply to the Manakov model directly. Derivation of dynamical equations for the interaction of Manakov solitons will be pursued elsewhere.

One of the main results of this paper is the proof of linear instability of stationary multivector-soliton bound states. The reason for this instability is largely due to phase-related unstable eigenvalues, as position-related eigenvalues can be made stable by proper arrangement of neighboring vector solitons, but phase-related eigenvalues cannot. Phase-related unstable eigenvalues, on the other hand, can trace their origins to phase invariances of the coupled NLS system (2.1) and (2.2). When phase invariance is broken in a wave system, then it becomes possible for stationary multipulse bound states to be actually stable. Such an example has been found in Ref. [25].

ACKNOWLEDGMENTS

This work was supported in part by the Air Force Office of Scientific Research under Contract No. F49620-99-1-0174, and by the National Science Foundation under Grant No. DMS-9971712.

[1] A. Hasegawa and Y. Kodama, *Solitons in Optical Communications* (Clarendon, Oxford, 1995).
[2] G. P. Agrawal, *Nonlinear Fiber Optics* (Academic Press, San Diego, 1989).
[3] H. Meng, G. Salamo, M. Shih, and M. Segev, Opt. Lett. **22**, 448 (1997).
[4] V. S. Gerdjikov, I. M. Uzunov, E. G. Evstatiev, and G. L. Diankov, Phys. Rev. E **55**, 6039 (1997).
[5] V. S. Gerdjikov, E. G. Evstatiev, D. J. Kaup, G. L. Diankov, and I. M. Uzunov, Phys. Lett. A **241**, 323 (1998).
[6] C. R. Menyuk, IEEE J. Quantum Electron. **QE-23**, 174 (1987).
[7] M. Haelterman, A. P. Sheppard, and A. W. Snyder, Opt. Lett. **18**, 1406 (1993).
[8] J. Yang, Physica D **108**, 92 (1997).
[9] J. Yang, Stud. Appl. Math. **100**, 127 (1998).
[10] A. Yew, B. Sandstede, and C. K. R. T. Jones, Phys. Rev. E **61**, 5886 (2000).
[11] Z. Chen, M. Acks, E. A. Ostrovskaya, and Y. S. Kivshar, Opt. Lett. **25**, 417 (2000).
[12] P. Kockaert and M. Haelterman, J. Opt. Soc. Am. B **16**, 732 (1999).
[13] E. A. Ostrovskaya, Y. S. Kivshar, D. V. Skryabin, and W. J. Firth, Phys. Rev. Lett. **83**, 296 (1999).
[14] V. I. Karpman and V. V. Solov'ev, Physica D **3**, 142 (1981).
[15] K. A. Gorshkov and L. A. Ostrovsky, Physica D **3**, 428 (1981).
[16] C. R. Menyuk, IEEE J. Quantum Electron. **QE-25**, 2674 (1989).
[17] V. E. Zakharov and A. B. Shabat, Zh. Éksp. Teor. Fiz. **61**, 118 (1971) [Sov. Phys. JETP **34**, 62 (1972)].
[18] S. V. Manakov, Zh. Éksp. Teor. Fiz. **65**, 1392 (1973) [Sov. Phys. JETP **38**, 248-253 (1974)].
[19] J. Yang and D. J. Kaup, SIAM (Soc. Ind. Appl. Math.) J. Appl. Math. **60**, 967 (2000).
[20] J. Yang, Stud. Appl. Math. **98**, 61 (1997).
[21] D. E. Pelinovsky and J. Yang, Stud. Appl. Math. **105**, 245 (2000).
[22] N. N. Akhmediev, A. V. Buryak, J. M. Soto-Crespo, and D. R. Andersen, J. Opt. Soc. Am. B **12**, 434 (1995).
[23] V. S. Gerdjikov, D. J. Kaup, I. M. Uzunov, and E. G. Evstatiev, Phys. Rev. Lett. **77**, 3943 (1996).
[24] J. M. Arnold, Phys. Rev. E **60**, 979 (1999).
[25] B. Sandstede, C. K. R. T. Jones, and J. C. Alexander, Physica D **106**, 167 (1997).